Low Temperature Physics/Fizika Nizkikh Temperatur, 2022, Vol. 48, No. 1, pp.

Comparative *ab initio* calculations of $SrTiO_3$, $BaTiO_3$, $PbTiO_3$, and $SrZrO_3$ (001) and (111) surfaces as well as oxygen vacancies

R. I. Eglitis[1], E. A. Kotomin[1], A. I. Popov[1], S. P. Kruchinin[2], and Ran Jia[1,3]

[1]*Institute of Solid State Physics, Riga LV 1063, Latvia*

[2]*Bogolyubov Institute for Theoretical Physics, Kyiv 03143, Ukraine*

[3]*Laboratory of Theoretical and Computational Chemistry, Institute of Theoretical Chemistry, Jilin University Changchun 130023, PR China*

E-mail: rieglitis@gmail.com

Received June 21, 2021, published online November 25, 2021

The paper presents and discusses the results of our performed *ab initio* calculations for perovskites $SrTiO_3$, $BaTiO_3$, $PbTiO_3$, and $SrZrO_3$ (001) and (111) surfaces by means of the hybrid B3PW or B3LYP description of exchange and correlation. According to our performed *ab initio* calculations for $SrTiO_3$, $BaTiO_3$, $PbTiO_3$, and $SrZrO_3$ (001) surfaces, in most cases, the upper layer atoms relax inwards, towards the bulk, and the second layer atoms relax upwards. The $SrTiO_3$, $BaTiO_3$, $PbTiO_3$, and $SrZrO_3$ (001) surface energies for AO and BO_2-terminations are almost equal. Just opposite, our calculated surface energies for both AO_3 and B-terminated (111) surfaces are quite different. Our calculated $SrTiO_3$, $BaTiO_3$, $PbTiO_3$, and $SrZrO_3$ (111) surface energies always are considerably larger than the (001) surface energies. The $SrTiO_3$, $BaTiO_3$, $PbTiO_3$, and $SrZrO_3$ bulk Ti-O (Zr-O) chemical bond covalency increases near their BO_2-terminated (001) as well as AO_3-terminated (111) surfaces. We discussed systematic trends in $SrTiO_3$, $BaTiO_3$, $PbTiO_3$, and $SrZrO_3$ bulk and (001) surface *F* center *ab initio* calculations.

Keywords: *Ab initio* calculations, ABO_3 perovskite surfaces, B3PW, B3LYP, Surface energies.

1. Introduction

Surface and interface phenomena taking place in the ABO_3 perovskites as well as their nanostructures, the complex nature of their surface and interface states, and the key mechanisms of surface electronic processes are very hot topics in nowadays modern condensed matter physics [1–12]. It is worth to note that $SrTiO_3$, $BaTiO_3$, $PbTiO_3$, and $SrZrO_3$ materials possess a huge number of technologically important applications, including, actuators, capacitors, charge storage devices as well as many others [13–17], for which the surface structure and quality play an important role. This is the key reason, why in the last quarter of century $SrTiO_3$, $BaTiO_3$, $PbTiO_3$, and $SrZrO_3$ neutral (001) surfaces were widely investigated around the globe both theoretically and experimentally [18–31]. Nevertheless, by means of the first principles calculations, it is much more difficult to calculate the polar and charged $SrTiO_3$, $BaTiO_3$, $PbTiO_3$, and $SrZrO_3$ (111) surfaces. This is the main reason, why the ABO_3 perovskite very complex, polar and charged (111) surfaces are considerably less studied than their neutral (001) surfaces [32–41].

It is worth to note, that all properties of the technologically important $SrTiO_3$, $BaTiO_3$, $PbTiO_3$, and $SrZrO_3$ perovskites are strongly affected by the point defects. The most common classical point defect in the $SrTiO_3$, $BaTiO_3$, $PbTiO_3$, and $SrZrO_3$ perovskites is the oxygen vacancy. It is well known, that the oxygen vacancy, or so called neutral *F* center (V_0) in ABO_3 perovskites captures two electrons. Theoretical and experimentall investigations of oxygen vacancies (*F* centers) in ABO_3 perovskites is a very hot topic, since the *F* center is a very well known classical point defect, which very strongly affects all technologically important properties of ABO_3 perovskites. While the *F* centers in $SrTiO_3$, $BaTiO_3$, $PbTiO_3$, and $SrZrO_3$ perovskite bulk are extensively studied world-wide both theoretically and experimentally [42–61], very small number of *ab initio* studies exist dealing with their (001) surface *F* centers [43, 53–56, 60, 62–64].

The goal of reported here work was to develop a unified theory, which describes systematic trends in $SrTiO_3$, $BaTiO_3$, $PbTiO_3$, and $SrZrO_3$ (001) and (111) surface and *F* centers in this perovskite bulk and on its (001) surfaces first principles calculations. *Ab initio* calculation results were carefully analyzed and systematic trends common to all $SrTiO_3$, $BaTiO_3$, $PbTiO_3$, and $SrZrO_3$ perovskite (001), (111) surface as well as bulk and (001) surface *F* center calculations were detected and systematized in a form easy accessible for a broad audience of readers.

2. *Ab initio* calculation method

2.1. $SrTiO_3$, $BaTiO_3$, $PbTiO_3$, *and* $SrZrO_3$ *(001) and (111) surface ab initio calculations*

We performed our *ab initio* calculations for $SrTiO_3$, $BaTiO_3$, $PbTiO_3$, and $SrZrO_3$ (001) and polar (111) surfaces and *F* centers using the B3PW [65] or B3LYP [66] hybrid exchange-correlation functionals and world well known CRYSTAL computer program package [67]. In contrast to the plane wave codes employed in a large number of previous studies [68, 69], the CRYSTAL program package [67] uses localized Gaussian type basis sets. We used, in our *ab initio* calculations, the basis sets developed for $SrTiO_3$, $BaTiO_3$, and $PbTiO_3$ in Ref. 70. Important privilege of the CRYSTAL computer program package [67] is its ability to perform *ab initio* computations for isolated two-dimensional slabs perpendicular to the $SrTiO_3$, $BaTiO_3$, $PbTiO_3$, and $SrZrO_3$ surfaces, without artificial periodicity in the *z* direction. The reciprocal space integration, in our *ab initio* calculations, were performed by sampling the Brillouin zone with an 8×8×1 times extended Pack–Monkhorst mesh for the $SrTiO_3$, $BaTiO_3$, $PbTiO_3$, and $SrZrO_3$ (001) surfaces as well as 8×8×8 mesh for those materials bulk. In order to reach very high accuracy of our computations, we used large enough tolerances of 7, 8, 7, 7, and 14 for the Coulomb overlap, Coulomb penetration, exchange overlap, first-exchange pseudo-overlap, and second-exchange pseudo-overlap, respectively [67].

We performed our *ab initio* calculations of ABO_3 perovskite (001) surfaces using symmetrical slabs containing nine alternating neutral AO and BO_2 layers. Our first slab was terminated by AO planes from both sides (Fig. 1). The AO-terminated, nine layer slab, consisted of 22 atoms containing supercell. The second our *ab initio* calculated slab from both sides was terminated by BO_2-planes and consisted of 23 atoms containing supercell (Fig. 2). In our *ab initio* calculations, both AO- and BO_2-terminated ABO_3 perovskite (001) slabs were non-stoichiometric [71]. Their unit cell equations are $A_5B_4O_{13}$ and $A_4B_5O_{14}$, respectively. In our $SrTiO_3$, $BaTiO_3$, $PbTiO_3$, and $SrZrO_3$ (001) surface calculations, since they consisted from neutral AO- or BO_2-terminated layers, we used the standard basis sets intended for ions [70]. Just opposite, in the case of $SrTiO_3$, $BaTiO_3$, $PbTiO_3$, and $SrZrO_3$ polar and charged (111) surfaces,

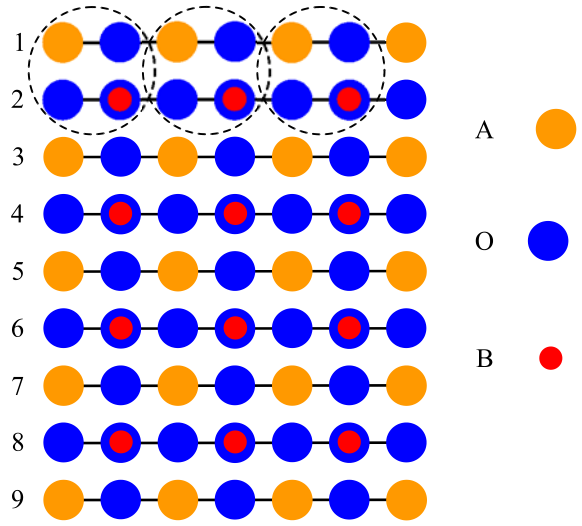

Fig. 1. Side view of the AO-terminated ABO_3 perovskite (001) surface which contains 9 layers.

since they consisted of charged layers (AO_3 or B) (Fig. 3), and assuming the classical ionic charges (+2*e*) for A, (+4*e*) for B and (-2*e*) for O, using nine-layer slabs (Fig. 4), we got charged AO_3 or B-terminated (111) surfaces. Taking into account that the supercell always should be neutral during the computations performed by the CRYSTAL computer code [67], we used the basis sets for neutral A, B, and O atoms [70]. Additional *ab initio* calculations details for $SrTiO_3$, $BaTiO_3$, $PbTiO_3$, and $SrZrO_3$ perovskite very complex, polar and charged (111) surfaces are described in references [34, 36, 38, 41, 45, 46]. With aim to describe

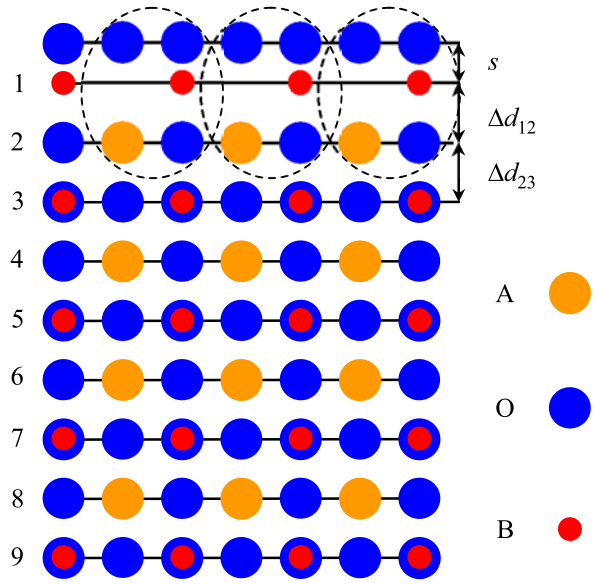

Fig. 2. Side view of the BO_2-terminated ABO_3 perovskite (001) surface containing the definitions of the surface rumpling and the nearest surface interplane distances.

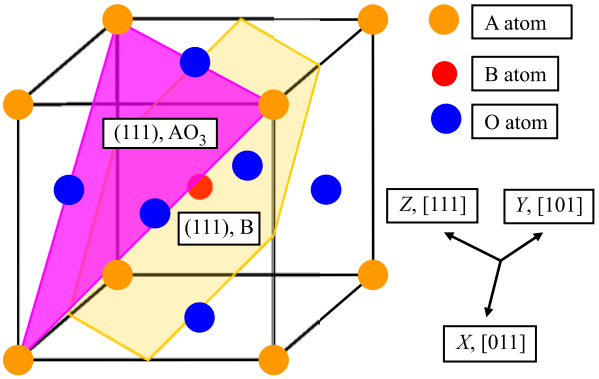

Fig. 3. Sketch of the cubic ABO_3 perovskite structure demonstrating two possible polar (111) surface terminations AO_3 and B.

the $SrTiO_3$, $BaTiO_3$, $PbTiO_3$, and $SrZrO_3$ perovskite chemical bonding and covalency effects, we employed the classical Mulliken population analysis for the effective atomic charges Q and other local properties of the perovskite electronic structure [72–74].

2.2. Surface energy calculations for $SrTiO_3$, $BaTiO_3$, $PbTiO_3$, *and* $SrZrO_3$ *(001) and (111) surfaces*

It is worth to note that the calculation methodology of ABO_3 perovskite (001) surface energies is already developed by us earlier [26]. Next, we calculated the $SrTiO_3$, $BaTiO_3$, $PbTiO_3$, and $SrZrO_3$ (111) surface energies using the following methodology. It is obvious that B- and AO_3-terminated ABO_3 perovskite (111) surfaces are mutually complementary. Therefore, it is clear that the cleavage energy is exactly the same for both AO_3- and B-terminated ABO_3 perovskite (111) surfaces. Thereby, the cleavage energy for the complementary surface $E_{cl}(AO_3 + B)$ can be computed from the total energies calculated for the unrelaxed slabs from the following equation:

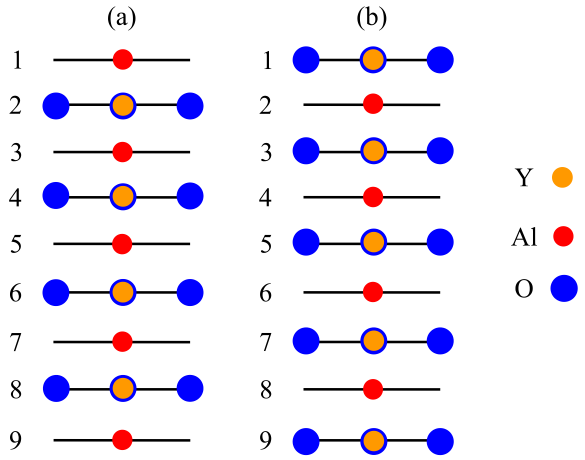

Fig. 4. Side views of the slab geometries used by us to study the ABO_3 perovskite polar (111) surfaces. a) Nonstoichiometric B-terminated nine-layer ABO_3 (111) slab and (b) nonstoichiometric AO_3-terminated nine-layer ABO_3 (111) slab.

$$E_{cl}\left(AO_3 + B\right) = ¼\left[E_{slab}^{unrel}\left(B\right) + E_{slab}^{unrel}\left(AO_3\right) - 9E_{bulk}\right], \quad (1)$$

where $E_{slab}^{unrel}(B)$ is our computed total energy of unrelaxed 21-atoms containing B-terminated ABO_3 (111) slab. $E_{slab}^{unrel}(AO_3)$ is our computed total energy for 24-atom AO_3-terminated ABO_3 (111) slab. E_{bulk} is the ABO_3 total bulk energy per formula unit containing 5-atoms in the cubic ABO_3 perovskite structure. In equation (1) factor 9 before the E_{bulk} is due to the fact that 21-atom B-terminated as well as 24-atom AO_3-terminated ABO_3 (111) slabs both together contain nine 5-atom ABO_3 bulk unit cells. Factor ¼ in the right side of the Eq. (1) means that totally four surfaces are created due to the crystal cleavage. The relevant relaxation energies for both B- and AO_3-terminated ABO_3 perovskite (111) surfaces can be computed by means of the following equation:

$$E_{rel}(\Omega) = ½\left[E_{slab}^{rel}(\Omega) - E_{slab}^{unrel}(\Omega)\right], \quad (2)$$

where Ω = B or AO_3 describes the ABO_3 perovskite (111) surface termination. $E_{slab}^{rel}(\Omega)$ is the B- or AO_3-terminated ABO_3 (111) slab total energy after the atomic relaxation. The $E_{slab}^{unrel}(\Omega)$ is the B- or AO_3-terminated ABO_3 (111) slab total energy before the atomic relaxation. The factor of ½ comes from the fact that two surfaces are created due to the crystal cleavage. Finally, the (111) surface energy is calculated as the sum of the cleavage and relaxation energies:

$$E_{surf}(\Omega) = E_{cl}\left(AO_3 + B\right) + E_{rel}(\Omega). \quad (3)$$

2.3. Ab initio calculation details of the bulk and (001) surface F centers in $SrTiO_3$, $BaTiO_3$, $PbTiO_3$, *and* $SrZrO_3$

All bulk *F* center *ab initio* calculations, for example for $SrZrO_3$ matrix, were performed using 3×3×3 times extended $SrZrO_3$ supercell containing 134 atoms and the single oxygen vacancy – *F* center (Fig. 5). Thereby, in our *ab initio* calculations, the bulk *F* center concentration was very low, only 1/81 or 1.23%. For the $SrZrO_3$ (001) surface calculations, containing the surface *F* center, we used a two-dimensional 11 layer slab model [71]. We allowed all atoms around the surface *F* center in the (001) slab to relax using a modified conjugate gradient algorithm [75, 76], with aim to locate a minimum on the potential energy surface.

We have employed a 3×3×1 times extended surface supercells, with one of the surface O atoms removed (Fig. 6), in order to calculate the surface *F* center properties located on the ZrO_2-terminated $SrZrO_3$ (001) surface. Thereby, the surface *F* center concentration in our calculations is equal to 1/18 or 5.56%. For the exact modelling of the bulk and (001) surface *F* centers, we add an additional basis function to the oxygen vacancy, corresponding to the so-called ghost-atom [67]. For this purpose, we have used exactly the same Gaussian-type functions as that employed for the O^{2-} ions of the $SrZrO_3$ perovskite bulk and ZrO_2-terminated (001) surface.

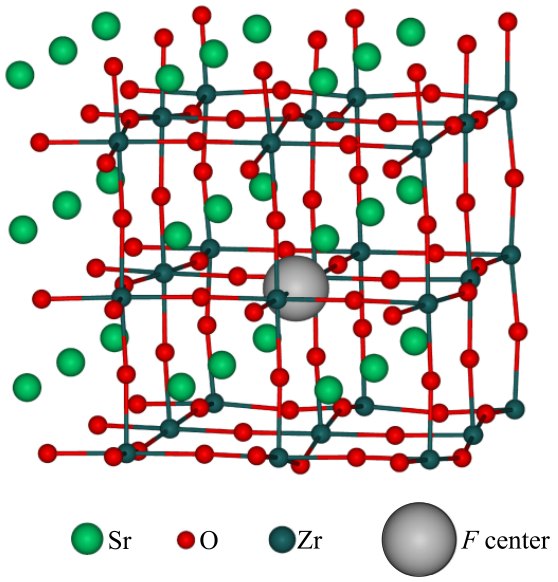

Fig. 5. Sketch of the cubic 3×3×3 times extended $SrZrO_3$ supercell containing the bulk *F* center.

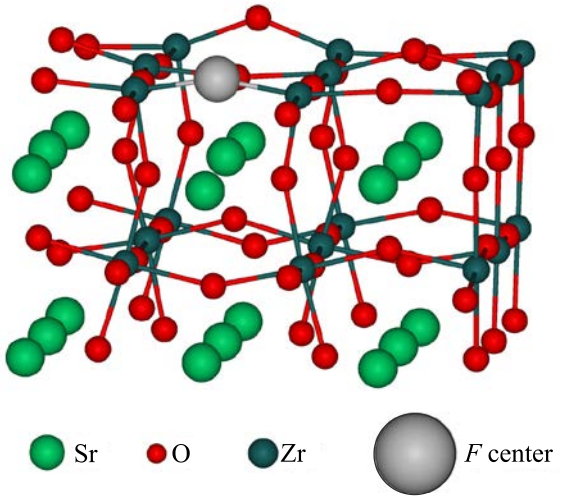

Fig. 6. Sketch of the surface *F* center located on the ZrO_2-terminated $SrZrO_3$ (001) surface.

3. Main *ab initio* calculation results

3.1. Ab initio calculation results for $SrTiO_3$, $BaTiO_3$, $PbTiO_3$, *and* $SrZrO_3$ *(001) and (111) surfaces*

As a starting point of our *ab initio* calculations, we calculated the $SrTiO_3$, $BaTiO_3$, $PbTiO_3$, and $SrZrO_3$ bulk lattice constants [28, 70, 77–79]. Namely, our by means of B3PW hybrid exchange-correlation functional calculated $SrTiO_3$, $BaTiO_3$, $PbTiO_3$, and $SrZrO_3$ bulk lattice constants are equal to 3.904, 4.008, 3.936, and 4.155Å, respectively. Our by B3LYP hybrid exchange-correlation functional calculated $SrTiO_3$, $BaTiO_3$, $PbTiO_3$, and $SrZrO_3$ bulk lattice constants are equal to 3.94, 4.04, 3.96, and 4.195 Å, respectively. Relevant experimental data [80–92], dealing with the $SrTiO_3$, $BaTiO_3$, $PbTiO_3$, and $SrZrO_3$ bulk lattice constants are collected in Table 1. We used our by means of B3PW hybrid exchange-correlatoion functional calculated theoretical bulk lattice constants as well as B3PW functional in all our future $SrTiO_3$, $BaTiO_3$, and PbTiO3 (001) surface calculations, whereas for SrZrO3 (001) surface calculations we used bulk lattice constant calculated by means of B3LYP functional as well as B3LYP functional for all future calculations. For $SrTiO_3$, $BaTiO_3$, $PbTiO_3$, and $SrZrO_3$ (111) surface calculations we always, in our future calculations used the lattice constants calculated by B3LYP hybrid exchange-correlation functional as well as B3LYP functional for our numerical calculations. Finally, just opposite, for *F* center calculations in $SrTiO_3$, $BaTiO_3$, $PbTiO_3$, and $SrZrO_3$ we used only the lattice constants calculated by B3PW functional as well as the B3PW functional for all numerical calculations. The hybrid exchange-correlation functionals B3PW and B3LYP, since they both are the hybrid-exchange correlation functionals as a rule gives results, which are very close, but, since they are the different functionals, the results, of course will be slightly different.

Our *ab initio* calculated atomic displacements for the $SrTiO_3$, $BaTiO_3$, $PbTiO_3$, and $SrZrO_3$ perovskite (001) surfaces are presented in Tables 2 and 3. According to the results of our *ab initio* calculations, most of atoms of the first (001) surface layer relax inwards towards the crystal bulk, whereas almost all atoms of the second (001) surface

Table 1. Experimental data for $SrTiO_3$, $BaTiO_3$, $PbTiO_3$, and $SrZrO_3$ perovskites, including band gap values and lattice constants

Material	Structure at RT	Band gap E_g, eV at RT	Transition *T*, K to cubic phase	Exp. lattice const., Å in cubic phase
$SrTiO_3$	Cubic	3.75 (direct); 3.25 (indirect) [80]	110 [81]	3.89845 (110 K) [82] 3.9053 (293 K) [83]
$BaTiO_3$	Tetragonal↔ Orthorhombic (278 K)	3.38 (// *c*); 3.27 (⊥ *c*) [84]	403 [81]	4.0037 (474 K) [85]
$PbTiO_3$	Tetragonal	3.4 [86, 87]	763 [88, 89]	3.970 (777 K) [89]
$SrZrO_3$	Orthorhombic	5.6 [90]	1433 [91] 1360 [92]	4.154 (1423 K) [92]

layer relax outwards, towards the vacuum (Table 2 and 3). The only two exceptions from this systematic trend are outward relaxations of the upper layer oxygen atom on the TiO_2-terminated $PbTiO_3$ (001) surface (Table 2) as well as the upper layer oxygen atom on the SrO-terminated $SrTiO_3$ (001) surface (Table 3). Finally, the second layer oxygen atom on the SrO-terminated $SrZrO_3$ (001) surface relax inwards by a very small relaxation magnitude, only (0.05% of a_0) (Table 3).

Table 2. Calculated displacements of TiO_2 or ZrO_2-terminated $SrTiO_3$, $BaTiO_3$, $PbTiO_3$, and $SrZrO_3$ (001) surface upper layer atoms (as a percentage of the bulk crystal lattice constant a_0). Positive (negative) values describe atomic displacements in the direction outwards (inwards) of the surface

Material		$SrTiO_3$	$BaTiO_3$	$PbTiO_3$	$SrZrO_3$
Termination		TiO_2	TiO_2	TiO_2	ZrO_2
Layer	Ion	Displ. (Δz)	Displ. (Δz)	Displ. (Δz)	Displ. (Δz)
1	B	–2.25	–3.08	–2.81	–1.38
	O	–0.13	–0.35	+0.31	–2.10
2	A	+3.55	+2.51	+5.32	+2.81
	O	+0.57	+0.38	+1.28	+0.91
3	B	–	–	–	–0.04
	O	–	–	–	–0.05

Table 3. Calculated displacements of SrO, BaO, PbO, and SrO-terminated $SrTiO_3$, $BaTiO_3$, $PbTiO_3$, and $SrZrO_3$ (001) surface upper layer atoms (as a percentage of the bulk crystal lattice constant a_0). Positive (negative) values describe atomic displacements in the direction outwards (inwards) of the surface

Material		$SrTiO_3$	$BaTiO_3$	$PbTiO_3$	$SrZrO_3$
Termination		SrO	BaO	PbO	SrO
Layer	Ion	Displ. (Δz)	Displ. (Δz)	Displ. (Δz)	Displ. (Δz)
1	A	–4.84	–1.99	–3.82	–7.63
	O	+0.84	–0.63	–0.31	–0.86
2	B	+1.75	+1.74	+3.07	+0.86
	O	+0.77	+1.40	+2.30	–0.05
3	A	–	–	–	–1.53
	O	–	–	–	–0.45

The relaxation magnitudes of the metal atoms on the upper and second layer of $SrTiO_3$, $BaTiO_3$, $PbTiO_3$, and $SrZrO_3$ (001) surfaces always are larger than the respective relaxation magnitudes of the oxygen atoms. The single exception from this rule is the ZrO_2-terminated $SrZrO_3$ (001) surface, where the upper layer oxygen atom inward displacement (2.10% of a_0) is larger than the Zr atom inward displacement (1.38% of a_0) (Table 2). It is worth to note that the third layer atom inward displacements for the ZrO_2-terminated $SrZrO_3$ (001) surface (0.04 and 0.05% of a_0, respectively) are already negligible (Table 2).

According to the results of our *ab initio* calculations (Table 4), for example, for $SrTiO_3$ (111) surfaces, the upper layer Ti atom for Ti-terminated $SrTiO_3$ (111) surface strongly (by 3.58% of a_0) relax inwards (Table 4). The second layer Sr atom moves inwards by even larger relaxation magnitude equal to 11.24% of a_0. Just opposite, the second layer O atom relaxes outwards by 1.53% of a_0 (Table 4). Finally, the outward displacement of the third layer Ti atom is already rather weak, less than 1% of a_0 (Table 4). For the SrO-terminated $SrTiO_3$ (111) surface the upper layer Sr atom moves outwards by 1.33% of a_0, but the upper layer O atom is displaced very slightly inwards by 0.03% of a_0. The second layer Ti atom outward displacement (1.81% of a_0) is slightly larger than the upper layer Sr atom relaxation (Table 4). Finally, both third layer Sr and O atoms relaxes inwards by a very small relaxation magnitude of (0.03% of a_0 and 0.26% of a_0, respectively) (Table 4).

Table 4. Calculated atomic displacements of Ti or Zr as well SrO_3, BaO_3, PbO_3, and SrO_3-terminated $SrTiO_3$, $BaTiO_3$, $PbTiO_3$, and $SrZrO_3$ (111) surface upper layer atoms (as a percentage of the bulk crystal lattice constant a_0). Positive (negative) values describe atomic displacements in the direction outwards (inwards) of the surface

Material		$SrTiO_3$	$BaTiO_3$	$PbTiO_3$	$SrZrO_3$
Termination		Ti-term.	Ti-term.	Ti-term.	Zr-term.
Layer	Ion	Displ. (Δz)	Displ. (Δz)	Displ. (Δz)	Displ. (Δz)
1	B	–3.58	–11.19	–7.57	–5.72
2	A	–11.24	–6.22	–10.09	–11.92
	O	+1.53	+2.74	–0.13	+0.79
3	B	+0.26	–0.25	+0.53	+1.53
Termination		SrO_3-term.	BaO_3-term.	PbO_3-term.	SrO_3-term.
Layer	Ion	Displ. (Δz)	Displ. (Δz)	Displ. (Δz)	Displ. (Δz)
1	A	+1.33	–1.24	+1.01	–0.74
	O	–0.03	–3.98	–2.52	–0.52
2	B	+1.81	+2.49	+0.02	+0.74
3	A	–0.03	+1.49	+1.26	–0.02
	O	–0.26	–0.25	+1.26	–0.18

As we can see from Table 4 that according to our performed *ab initio* calculations for Ti or Zr-terminated $SrTiO_3$, $BaTiO_3$, $PbTiO_3$, and $SrZrO_3$ (111) surfaces all upper two layer metal atoms relax inwards. The largest inward relaxation magnitude is for Ti-terminated $BaTiO_3$ (111) surface upper layer Ti atom (11.19% of a_0) and for Zr-terminated $SrZrO_3$ (111) surface second layer Sr atom (11.92% of a_0). It is worth to note that for the SrO_3, BaO_3, PbO_3 and SrO_3-terminated $SrTiO_3$, $BaTiO_3$, $PbTiO_3$, and $SrZrO_3$ (111) surfaces all upper layer oxygen atoms relax inwards, whereas all second layer metal atoms relax upwards (Table 4).

Our *ab initio* calculated surface energy for the SrO_3-terminated $SrTiO_3$ (111) surface is equal to 6.30 eV and thereby it by 1.31 eV exceeds the surface energy for Ti-terminated $SrTiO_3$ (111) surface 4.99 eV (Table 5). Calculated SrO_3 and Ti-terminated $SrTiO_3$ (111) surface energies (6.30 and 4.99 eV) are considerably larger than the SrO and TiO_2-terminated $SrTiO_3$ (001) surface energies 1.15 and 1.23 eV, respectively (Table 5). Also for another our calculated $BaTiO_3$, $PbTiO_3$, and $SrZrO_3$ perovskites, their (111) surface energies for both AO_3 and B-terminations (Table 5) are always larger than their relevant surface energies for both AO and BO_2-terminated (001) surfaces. As we can see from Table 5 that the AO_3-terminated perovskite (111) surface energies are always larger than the B-terminated (111) surface energies for the $SrTiO_3$, $BaTiO_3$, $PbTiO_3$, and $SrZrO_3$ perovskites.

Table 5. Ab initio calculated surface energies for SrTiO3, BaTiO3, PbTiO3 and SrZrO3 (001) and (111) surfaces (in electron volt per surface cell)

Material	Termination	E_{surf} (001)	Termination	E_{surf} (111)
$SrTiO_3$	SrO-term.	1.15	SrO_3-term.	6.30
	TiO_2-term.	1.23	Ti-term.	4.99
$BaTiO_3$	BaO-term.	1.19	BaO_3-term.	8.40
	TiO_2-term.	1.07	Ti-term.	7.28
$PbTiO_3$	PbO-term.	0.83	PbO_3-term.	8.11
	TiO_2-term.	0.74	Ti-term.	6.14
$SrZrO_3$	SrO-term.	1.13	SrO_3-term.	9.45
	ZrO_2-term.	1.24	Zr-term.	7.98

As we can see from Table 6, the effect of the strong Ti-O (Zr-O) chemical bond covalency was already well pronounced for $SrTiO_3$, $BaTiO_3$, $PbTiO_3$, and $SrZrO_3$ crystals in the bulk (+0.088*e*, +0.098*e*, +0.098*e*, and +0.092*e*). As follows from the chemical bond covalency analysis (Table 6), for all four our *ab initio* computed $SrTiO_3$, $BaTiO_3$, $PbTiO_3$, and $SrZrO_3$ perovskites, the main effect for polar (111) surfaces is the strengthening of the Ti-O (Zr-O) chemical bond covalency near the SrO_3 (+0.098*e*), BaO_3 (+0.118*e*), PbO_3 (+0.116*e*), and SrO_3-terminated (+0.098*e*) surfaces. Nevertheless, it is worth to note that in most cases, the strongest Ti-O (Zr-O) chemical bond covalency, according to our *ab initio* calculations, is observed near the TiO_2 or ZrO_2-terminated $SrTiO_3$ (+0.118*e*), $BaTiO_3$ (+0.126*e*), $PbTiO_3$ (+0.114*e*), and $SrZrO_3$ (+0.114*e*) (001) surfaces, respectively. We used the Mulliken population analysis for the description of the chemical bond covalency [72–74].

3.2. Ab initio calculation results for $SrTiO_3$, $BaTiO_3$, $PbTiO_3$, *and* $SrZrO_3$ *bulk and (001) surface F centers*

As a starting point of our *F* center *ab initio* calculations in the $BaTiO_3$ bulk, we optimized the equilibrium geometry

Table 6. *Ab initio* calculated effective atomic charges (in *e*) as well B-O chemical bond populations in $SrTiO_3$, $BaTiO_3$, $PbTiO_3$, and $SrZrO_3$ perovskite bulk, BO_2-terminated (001) and AO_3-terminated (111) surfaces (in *e*)

Effective atomic charges	$SrTiO_3$	$BaTiO_3$	$PbTiO_3$	$SrZrO_3$
A	+1.871	+1.797	+1.354	+1.880
B	+2.351	+2.367	+2.341	+2.174
O	–1.407	–1.388	–1.232	–1.351
B–O bond population				
Bulk	+0.088	+0.098	+0.098	+0.092
BO_2-terminated (001)	+0.118	+0.126	+0.114	+0.114
AO_3-terminated (111)	+0.098	+0.118	+0.116	+0.098

surrounding a single *F* center located in the center of a 3×3×3 times extended supercell (Fig. 5). We computed the geometry relaxation of the nearest to the bulk *F* center Ti, O, and Ba atoms along the directions in the $BaTiO_3$ matrix allowed by the crystal symmetry. Our *ab initio* computed nearest atom displacements surrounding the $BaTiO_3$ bulk *F* center are collected in Table 7 and compared with the results obtained for $SrTiO_3$, $PbTiO_3$, and $SrZrO_3$ perovskites. Namely, the two nearest to the *F* center in the $BaTiO_3$ Ti atoms are repulsed by 1.06% of the a_0. The outward displacement of the two nearest to the bulk *F* center B atoms is calculated by us also for $SrTiO_3$, $PbTiO_3$, and $SrZrO_3$ perovskites (Table 7) [53–56] and seems that it is typical also for another ABO_3 perovskites.

As a next step, we computed the $BaTiO_3$ effective atomic charge inside the bulk *F* center defect. The charge of this bulk $BaTiO_3$ *F* center is only –1.103*e*, which is much smaller amount than expected from the O atom charge in the perfect $BaTiO_3$ crystal (–1.388*e*) (Tables 6 and 7). Also for $SrTiO_3$, $PbTiO_3$, and $SrZrO_3$ perovskites (–1.1*e*, –0.85*e*, –1.25*e*, respectively) (Table 7) considerably smaller charge are located in the neutral oxygen vacancy than that expected from the O atom charge in the perfect $SrTiO_3$, $PbTiO_3$, and $SrZrO_3$ perovskites (–1.407*e*, –1.232*e*, and –1.351*e*, respectively). Another key effect in $BaTiO_3$ is a very large increase of the chemical bond covalency between the *F* center and its two nearest neighbor Ti atoms equal to 0.320*e*, while in the perfect $BaTiO_3$ bulk the chemical bond population between the O and Ti atoms was only (0.098*e*). Such effect, the increase of the chemical bond covalency between the bulk *F* center and its nearest metal atoms is observed also in another ABO_3 perovskites [53, 54] as well as in CaF_2 and MgF_2 [93, 94].

Finally, we calculated the *F* center formation energy in the $BaTiO_3$ bulk. The formation energy of the *F* center

Table 7. Ab initio calculated $SrTiO_3$, $BaTiO_3$, $PbTiO_3$, and $SrZrO_3$ bulk and (001) surface *F* center main characteristics [53–56]. The sign "–" before relaxed coordinates means sphere contraction

Bulk *F* center	$SrTiO_3$	$BaTiO_3$	$PbTiO_3$	$SrZrO_3$
F center charge	–1.1 *e*	–1.103 *e*	–0.85 *e*	–1.25 *e*
F under CB, eV	0.69	0.23	0.96	1.12
Formation energy, eV	7.1	10.3	7.82	7.55
B relaxation, % of a_0	7.76	1.06	6.5	3.68
O relaxation, % of a_0	–7.79	–0.71	–	–2.63
A relaxation, % of a_0	3.94	–0.08	–	0.46
Surface *F* center	$SrTiO_3$	$BaTiO_3$	$PbTiO_3$	$SrZrO_3$
Surface termination (001)	TiO_2-term.	BaO-term.	–	ZrO_2-term.
F center charge	–	–1.052 *e*	–	–1.10 *e*
F under CB, eV	0.25	0.07	–	0.93
Formation energy, eV	6.22	10.2	–	7.52
B relaxation, % of a_0	14	0.1	–	9.17
O relaxation, % of a_0	–8	–1.4	–	–4.16
A relaxation, % of a_0	–	1.0	–	7.68

in the $BaTiO_3$ bulk was calculated by means of the following equation:

$$E_{\text{form}}^{(F)} = E_{\text{oxy}} + E_F - E_{\text{perf}} \quad (4)$$

where E_{oxy} is our calculated total energy for a single oxygen atom. In order to calculate the single oxygen atom energy, we started our calculations from the O_2 molecule. Next, we strongly increased the distance between the two atoms of O_2 molecule, in order to eliminate any interaction between them. Finally, the single oxygen atom energy is the O_2 molecule energy, when the distance between the O atoms is maximally increased, divided by the number of atoms in the oxygen molecule equal to two. E_{perf} and E_F are calculated total energies for the perfect $BaTiO_3$ bulk, and the $BaTiO_3$ bulk containing the *F* center defect, respectively. Our calculated *F* center formation energy in the $BaTiO_3$ bulk, according to Eq. (1) is equal to 10.3 eV. The formation energies of the *F* center in $SrTiO_3$, $PbTiO_3$, and $SrZrO_3$ bulk are equal to (7.1, 7.82, and 7.55 eV, respectively). It is worth to note that the Eq. (4) works perfectly also for another class of materials, like CaF_2, BaF_2, and SrF_2. Our *ab initio* calculated *F* center (fluorine vacancy) formation energies in CaF_2 (7.87 eV), BaF_2 (7.82 eV), and SrF_2 (10.33 eV) [43, 74, 94] are comparable with our *ab initio* calculated *F* center formation energies in ABO_3 perovskites [53, 54].

As we can see from Table 7 that repulsion of Ti atom from the *F* center located on TiO_2-terminated $SrTiO_3$ (001) surface (14% of a_0) is considerably larger than it was for Ti repulsion from the *F* center located in the $SrTiO_3$ perovskite bulk (7.76% of a_0). Also Zr atom repulsion from the *F* center located on the ZrO_2-terminated $SrZrO_3$ (001) surface (9.17% of a_0) is much larger than the Zr atom repulsion from the $SrZrO_3$ bulk *F* center (3.68% of a_0).

As we can see from Table 7 that for the $BaTiO_3$ perovskite surface *F* center located on the BaO-terminated (001) surface only (–1.052*e*) is localized inside the oxygen vacancy. Also for the *F* center located on the ZrO_2-terminated $SrZrO_3$ (001), only (–1.10*e*) is localized inside the oxygen vacancy, which is less than for the *F* center located in the $SrZrO_3$ bulk (–1.25*e*). Finally, our calculated formation energy of *F* center located on the BaO-terminated $BaTiO_3$ (001) surface (10.2 eV) is only by 0.1 eV smaller than the *F* center formation energy in the $BaTiO_3$ perovskite bulk (10.3 eV) (Table 7).

4. Conclusions

With a few exceptions, the $SrTiO_3$, $BaTiO_3$, $PbTiO_3$, and $SrZrO_3$ perovskite neutral (001) surface all upper layer atoms relax inwards, whereas all second layer atoms relax outwards. As we can see from Table 4 that according to our performed *ab initio* calculations for Ti or Zr-terminated $SrTiO_3$, $BaTiO_3$, $PbTiO_3$, and $SrZrO_3$ (111) surfaces all upper two layer metal atoms relax inwards. It is worth to note that for the SrO_3, BaO_3, PbO_3, and SrO_3-terminated $SrTiO_3$, $BaTiO_3$, $PbTiO_3$, and $SrZrO_3$ (111) surfaces all upper layer oxygen atoms relax inwards, whereas all second layer metal atoms relax upwards (Table 4). The $SrTiO_3$, $BaTiO_3$, $PbTiO_3$, and $SrZrO_3$ neutral (001) surface energies for both terminations AO and BO_2 are almost equal. Just opposite, the $SrTiO_3$, $BaTiO_3$, $PbTiO_3$, and $SrZrO_3$ (111) surface energies for AO_3 and B-terminations are quite different. Moreover, the ABO_3 perovskite (111) surface energies always are considerably larger than the (001) surface energies (Table 5). As follows from the chemical bond covalency analysis (Table 6), for all 4 our *ab initio* computed perovskites, the main effect is the strengthening of the Ti-O (Zr-O) chemical bond covalency near the SrO_3

(+0.098*e*), BaO_3 (+0.118*e*), PbO_3 (+0.116*e*), and SrO_3-terminated (+0.098*e*) $SrTiO_3$, $BaTiO_3$, $PbTiO_3$, and $SrZrO_3$ (111) surfaces in comparison to the bulk values. Nevertheless, it is worth to note that in most cases, the strongest Ti-O (Zr-O) chemical bond covalency, according to our *ab initio* calculations, is observed near the neutral TiO_2 or ZrO_2-terminated $SrTiO_3$ (+0.118*e*), $BaTiO_3$ (+0.126*e*), $PbTiO_3$ (+0.114*e*), and $SrZrO_3$ (+0.114*e*) (001) surfaces (Table 6).

The *ab initio* computed atomic displacements of the nearest neighbor atoms around the $SrTiO_3$, $BaTiO_3$, and $SrZrO_3$ (001) surface *F* centers, in most cases, are larger than the relevant nearest neighbor atomic displacements around the bulk *F* centers. It is worth to note that the theory for development of defects in time was developed by Kotomin *et al*. [95]. As a rule, the $SrTiO_3$, $BaTiO_3$, and $SrZrO_3$ (001) surface *F* center electrons are considerably more delocalized, namely, less amount of electrons are trapped inside the oxygen vacancy, than in the bulk *F* center case. The energy difference between the $SrTiO_3$, $BaTiO_3$, and $SrZrO_3$ typically smaller (001) surface *F* center formation energies as well as larger bulk *F* center formation energies triggers the segregation of *F* centers from bulk towards the (001) surface of these perovskites. The $SrTiO_3$, $BaTiO_3$, and $SrZrO_3$ (001) surface *F* center induced defect levels in the band gap is located closer to the conduction band bottom than it was for the bulk *F* centers in these perovskites (Table 7).

In conclusion, we would like to emphasize that the results of this work are interesting and important not only for understanding the surface properties of simple cubic perovskites, but more importantly, allows a more detailed understanding of the corresponding surface properties of complex oxide materials [96–98], which are currently of great practical interest.

Acknowledgments

This research was partly funded by the Latvian Council of Science project No. LZP-2018/1-0147 (E. Kotomin) as well as project No. LZP-2020/2-0009 (for R. Eglitis). S. P. Kruchinin acknowledges support by the National Academy of Sciences of Ukraine project "Functional properties of materials prospective for nanotechnologies" (No. 0120U100858). The Institute of Solid State Physics University of Latvia (Latvia) as the Centre of Excellence has received funding from the European Union Horizon 2020 Framework Programme H2020 – WIDESPREAD01-2016-2017-Teamimg Phase2 under Grant Agreement No. 739508, project CAMART2.

1. R. A. P. Ribeiro, J. Andres, E. Longo, and S. R. Lazaro, *Appl. Surf. Sci.* **452**, 463 (2018).
2. V. M. Longo, L. S. Cavalcante, A. T. Figueiredo, and L. P. S. Santos, *Appl. Phys. Lett.* **90**, 091906 (2007).
3. A. S. Farlenkov, M. V. Ananyev, V. A. Eremin, N. M. Porotnikova, E. K. Kurumchin, and B. T. Melekh, *Solid State Ion.* **290**, 108 (2016).
4. R. I. Eglitis, J. Kleperis, J. Purans, A. I. Popov, and R. Jia, *J. Mater. Sci.* **55**, 203 (2020).
5. V. S. Vikhnin, H. M. Liu, W. Y. Jia, S. Kapphan, R. Eglitis, and D. Usvyat, *J. Lumin.* **83–84**, 109 (1999).
6. S. Piskunov and R.I. Eglitis, *Solid State Ion.* **274**, 29 (2015).
7. A. A. Kurteeva, N. M. Bogdanovich, D. I. Bronin, N. M. Porotnikova, G. K. Vdovin, A. A. Pankratov, S. M. Beresnev, and L. A. Kuzmina, *Russ. J. Electrochem.* **46**, 811 (2010).
8. I. Z. Zhumatayeva, I. E. Kenzhina, A. L. Kozlovskiy, and M. V. Zdorovets, *J. Mater. Sci.: Mater. Electron.* **31**, 6744 (2020).
9. R. I. Eglitis and A. I. Popov, *Nucl. Instrum. Methods Phys. Res. B* **434**, 1 (2018).
10. K. Dukenbayev, A. Kozlovskiy, I. Kenzhina, A. Berguzinov, and M. Zdorovets, *Mater. Res. Express* **6**, 046309 (2019).
11. V. Dimza, A. I. Popov, L. Lace, M. Kundzins, K. Kundzins, M. Antonova, and M. Livins, *Curr. Appl. Phys.* **17**, 169 (2017).
12. R. I. Eglitis, E. A. Kotomin, and G. Borstel, *J. Phys.: Condens. Matter* **12**, L431 (2000).
13. H. Y. Hwang, Y. Iwasa, M. Kawasaki, B. Keimer, N. Nagaosa, and Y. Tokura, *Nat. Mater.* **11**, 103 (2012).
14. L. Grigorjeva, D. K. Millers, V. Pankratov, R. T. Williams, R. I. Eglitis, E. A. Kotomin, and G. Borstel, *Solid State Commun.* **129**, 691 (2004).
15. R. I. Eglitis, E. A. Kotomin, V. A. Trepakov, S. E. Kapphan, and G. Borstel, *J. Phys.: Condens. Matter* **14**, L647 (2002).
16. C. Franchini, M. Reticcioli, M. Setvin, and U. Diebold, *Nat. Rev. Mater.* **6**, 560 (2021).
17. M. Zhong, W. Zeng, F. S. Liu, B. Tang, and Q. J. Liu, *Surf. Interface Anal.* **51**, 1021 (2019).
18. R. I. Eglitis, J. Purans, J. Gabrusenoks, A. I. Popov, and R. Jia, *Crystals* **10**, 745 (2020).
19. R. I. Eglitis, J. Purans, and R. Jia, *Crystals* **11**, 455 (2021).
20. J. R. Sambrano, V. M. Longo, E. Longo, and C. A. Taft, *J. Mol. Struct. THEOCHEM* **813**, 49 (2007).
21. R. Eglitis and S. P. Kruchinin, *Mod. Phys. Lett. B* **34**, 2040057 (2020).
22. J. S. Kim, J. H. Wang, B. K. Kim, and Y. C. Kim, *Solid State Ion.* **275**, 19 (2015).
23. X. Guo, J. Ge, F. Ponchel, D. Remiens, Y. Chen, X. Dong, and G. Wang, *Thin Solid Films* **632**, 93 (2017).
24. G. Borstel, R. I. Eglitis, E. A. Kotomin, and E. Heifets, *Phys. Status Solidi B* **236**, 253 (2003).
25. H. S. Wei, J. Y. Cai, Y. Zhang, X. R. Zhang, E. A. Baranova, J. W. Cui, Y. Wang, X. Shu, Y. Q. Qin, J. Q. Liu, and Y. C. Wu, *RSC Adv.* **10**, 42619 (2020).
26. E. Heifets, R. I. Eglitis, E. A. Kotomin, J. Maier, and G. Borstel, *Phys. Rev. B* **64**, 235417 (2001).
27. Y. Li, J. Yang, Y. A. Zhu, Z. J. Sui, X. G. Zhou, D. Chen, and W. K. Yuan, *Phys. Chem. Chem. Phys.* **21**, 12859 (2019).

28. R. I. Eglitis and D. Vanderbilt, *Phys. Rev. B* **76**, 155439 (2007).
29. H. J. Chun, H. K. Kim, Y. Yoon, and S. C. Park, *Surf. Sci.* **703**, 121737 (2021).
30. N. V. Krainyukova, V. O. Hamalii, A. V. Peschanskii, A. I. Popov, and E. A. Kotomin, *Fiz. Nizk. Temp.* **46**, 877 (2020) [*Low Temp. Phys.* **46**, 740 (2020)].
31. V. O. Hamalii, A. V. Peschanskii, A. I. Popov, and N. V. Krainyukova, *Fiz. Nizk. Temp.* **46**, 1377 (2020) [*Low Temp. Phys.* **46**, 1170 (2020)].
32. S. Okamoto, W. Zhu, Y. Nomura, R. Arita, D. Xiao, and N. Nagaosa, *Phys. Rev. B* **89**, 195121 (2014).
33. S. Okamoto and D. Xiao, *J. Phys. Soc. Jpn.* **87**, 041006 (2018).
34. R. I. Eglitis, *Appl. Surf. Sci.* **358**, 556 (2015).
35. B. C. Russell and M. R. Castell, *J. Phys. Chem. C* **112**, 6538 (2008).
36. R. I. Eglitis, *Phys. Status Solidi B* **252**, 635 (2015).
37. L. Miao, R. Du, Y. Yin, and Q. Li, *Appl. Phys. Lett.* **109**, 261604 (2016).
38. R. I. Eglitis, *Ferroelectrics* **483**, 53 (2015).
39. Y. Zhu, P. A. Salvador, and G. S. Rohrer, *Chem. Mater.* **28**, 5155 (2016).
40. T. Bolstad, K. Kjærnes, K. Raa, R. Takahashi, M. Lippmaa, and T. Tybell, *Mater. Res. Express* **6**, 056409 (2019).
41. R. I. Eglitis, J. Purans, A. I. Popov, and Ran Jia, *Int. J. Mod. Phys. B* **33**, 1950390 (2019).
42. A. I. Popov, E. A. Kotomin, and J. Maier, *Nucl. Instr. Meth. B* **268**, 3084 (2010).
43. R. Eglitis, A. I. Popov, J. Purans, and R. Jia, *Fiz. Nizk. Temp.* **46**, 1418 (2020) [*Low Temp. Phys.* **46**, 1206 (2020)].
44. L. L. Rusevich, E. A. Kotomin, G. Zvejnieks, and A. I. Popov, *Fiz. Nizk. Temp.* **46**, 1394 (2020) [*Low Temp. Phys.* **46**, 1185 (2020)].
45. R. I. Eglitis, *Int. J. Mod. Phys. B* **28**, 1430009 (2014).
46. R. I. Eglitis and A. I. Popov, *J. Nano- Electron. Phys.* **11**, 01001 (2019).
47. E. A. Kotomin and A. I. Popov, *Nucl. Instr. Meth. B* **141**, 1 (1998).
48. H. Donnerberg and A. Birkholz, *J. Phys.: Condens. Matter* **12**, 8239 (2000).
49. J. J. Brown, Z. Ke, W. Geng, and A. J. Page, *J. Phys. Chem. C* **122**, 14590 (2018).
50. M. Q. Cai, Y. J. Zhang, Z. Yin, and M. Zhang, *Phys. Rev. B* **72**, 075406 (2005).
51. M. Arrigoni, T. S. Bjørnheim, E. Kotomin, and J. Maier, *Phys. Chem. Chem. Phys.* **18**, 9902 (2016).
52. C. Duque and A. Stashans, *Physica B* **336**, 227 (2003).
53. R. I. Eglitis and S. Piskunov, *Comput. Condens. Matter* **7**, 1 (2016).
54. M. Sokolov, R. I. Eglitis, S. Piskunov, and Y. F. Zhukovskii, *Int. J. Mod. Phys. B* **31**, 1750251 (2017).
55. J. Carrasco, F. Illas, N. Lopez, E. A. Kotomin, Y. F. Zhukovskii, R. A. Evarestov, Y. A. Mastrikov, S. Piskunov, and J. Maier, *Phys. Rev. B* **73**, 064106 (2006).
56. Y. F. Zhukovskii, E. A. Kotomin, S. Piskunov, and D. E. Ellis, *Solid State Commun.* **149**, 1359 (2009).
57. R. I. Eglitis, E. A. Kotomin, G. Borstel, S. E. Kapphan, and V. S. Vikhnin, *Comput. Mater. Sci.* **27**, 81 (2003).
58. I. I. Leonidov, V. I. Tsidilkovski, E. S. Tropin, M. I. Vlasov, and L. P. Putilov, *Mater. Lett.* **212**, 336 (2018).
59. H. Tan, Z. Zhao, W. B. Zhu, E. N. Coker, B. Li, M. Zheng, W. Yu, H. Fan, and Z. Sun, *ACS Appl. Mater. Interfaces* **6**, 19184 (2014).
60. E. A. Kotomin, S. Piskunov, Y. F. Zhukovskii, R. I. Eglitis, A. Gopejenko, and D. E. Ellis, *Phys. Chem. Chem. Phys.* **10**, 4258 (2008).
61. Q. C. Zhao, H. L. Gong, X. H. Wang, and L. T. Li, *Phys. Status Solidi A* **215**, 1800168 (2018).
62. R. Shimizu, K. Iwaya, T. Ohsawa, S. Shiraki, T. Hasegawa, T. Hashizume, and T. Hitosugi, *Appl. Phys. Lett.* **100**, 263106 (2012).
63. K. Takeyasu, K. Fukada, M. Matsumoto, and K. Fukutani, *J. Phys.: Condens. Matter* **25**, 162202 (2013).
64. Y. L. Li, D. N. Zhang, S. B. Qu, M. Yang, and Y. P. Feng, *Surf. Sci.* **641**, 37 (2015).
65. J. P. Perdew and Y. Wang, *Phys. Rev. B* **45**, 13244 (1992).
66. C. Lee, W. Yang, and R. G. Parr, *Phys. Rev. B* **37**, 785 (1988).
67. V. R. Saunders, R. Dovesi, C. Roetti, N. Causa, N. M. Harrison, R. Orlando, and C. M. Zicovich-Wilson, *CRYSTAL-2014 User Manual*, University of Torino, Italy (2014).
68. R. E. Cohen, *J. Phys. Chem. Solids* **57**, 1393 (1996).
69. R. E. Cohen, *Ferroelectrics* **194**, 323 (1997).
70. S. Piskunov, E. Heifets, R. I. Eglitis, and G. Borstel, *Comput. Mater. Sci.* **29**, 165 (2004).
71. P. W. Tasker, *J. Phys. C* **12**, 4977 (1979).
72. I. Mayer, *Int. J. Quantum. Chem.* **26**, 151 (1984).
73. R. C. Bochicchio and H. F. Reale, *J. Phys. B* **26**, 4871 (1993).
74. H. Shi, L. Chang, R. Jia, and R. I. Eglitis, *J. Phys. Chem. C* **116**, 4832 (2012).
75. H. B. Schlegel, *J. Comput. Chem.* **3**, 214 (1982).
76. B. Civalleri, P. D'Arco, R. Orlando, V. R. Saunders, and R. Dovesi, *Chem. Phys. Lett.* **348**, 131 (2001).
77. S. Piskunov, E. A. Kotomin, E. Heifets, J. Maier, R. I. Eglitis, and G. Borstel, *Surf. Sci.* **575**, 75 (2005).
78. R. I. Eglitis and D. Vanderbilt, *Phys. Rev. B* **77**, 195408 (2008).
79. R. I. Eglitis and M. Rohlfing, *J. Phys.: Condens. Matter* **22**, 415901 (2010).
80. K. van Benthem, C. Elsässer, and R. H. French, *J. Appl. Phys.* **90**, 6156 (2001).
81. B. Meyer, J. Padilla, and D. Vanderbilt, *Faraday Discuss.* **114**, 395 (1999).
82. M. Sato, Y. Soejima, N. Ohama, A. Okazaki, H. J. Scheel, and K. A. Müller, *Phase Trans.* **5**, 207 (1985).
83. J. G. Bednorz and H. J. Scheel, *J. Cryst. Growth* **41**, 5 (1977).
84. S. H. Wemple, *Phys. Rev. B* **2**, 2679 (1970).
85. J. W. Edwards, R. Speiser, and H. L. Johston, *J. Amer. Chem. Soc.* **73**, 2934 (1951).
86. J. Robertson, *J. Vac. Sci. Technol. B* **18**, 1785 (2000).

87. C. H. Peng, J. F. Chang, and S. Desu, *Mater. Res. Soc. Symp. Proc.* **243**, 21 (1992).
88. R. J. Nelmes and W. F. Kuhs, *Solid State Commun.* **54**, 721 (1985).
89. S. A. Mabud and A. M. Glazer, *J. Appl. Cryst.* **12**, 49 (1979).
90. Y. S. Lee, J. S. Lee, T. W. Noh, D. Y. Byun, K. S. Yoo, K. Yamaura, and E. Takayama-Muromachi, *Phys. Rev. B* **67**, 113101 (2003).
91. M. Yoshino, H. Yukawa, and M. Morinaga, *Mater. Trans.* **45**, 2056 (2004).
92. B. J. Kennedy, C. J. Howard, and B. C. Chakoumakos, *Phys. Rev. B* **59**, 4023 (1999).
93. A. F. Fix, F. U. Abuova, E. A. Kotomin, and A. T. Akilbekov, *Phys. Scr.* **86**, 035304 (2012).
94. H. Shi, R. Jia, and R. I. Eglitis, *Solid State Ion.* **187**, 1 (2011).
95. E. A. Kotomin, A. I. Popov, and R. I. Eglitis, *J. Phys.: Condens. Matter* **4**, 5901 (1992).
96. A. S. Farlenkov, M. V. Ananyev, V. A. Eremin, N. M. Porotnikova, and E. K. Kurumchin, *Fuel Cells* **15**, 131 (2015).
97. N. M. Porotnikova, V. A. Eremin, A. S. Farlenkov, E. K. Kurumchin, E. A. Sherstobitova, D. I. Kochubey, and M. V. Ananyev, *Catal. Lett.* **148**, 2839 (2018).
98. D. A. Osinkin, A. V. Khodimchuk, N. M. Porotnikova, N. M. Bogdanovich, A. V. Fetisov, and M. V. Ananyev, *Energies* **13**, 250 (2020).

Порівняльні *ab initio* розрахунки для $SrTiO_3$, $BaTiO_3$, $PbTiO_3$ та $SrZrO_3$ (001) і (111) поверхонь, а також вакансій кисню

R. I. Eglitis, E. A. Kotomin, A. I. Popov, S. P. Kruchinin, Ran Jia

Представлено та обговорено результати проведених *ab initio* розрахунків для перовскітів $SrTiO_3$, $BaTiO_3$, $PbTiO_3$ та $SrZrO_3$ (001) і (111) поверхонь за допомогою гібридного опису обміну та кореляції B3PW або B3LYP. Згідно з проведеними *ab initio* розрахунками для $SrTiO_3$, $BaTiO_3$, $PbTiO_3$ та $SrZrO_3$ (001) поверхонь, у більшості випадків атоми поверхневого шару релаксують всередину, а атоми другого шару релаксують угору. Поверхневі енергії $SrTiO_3$, $BaTiO_3$, $PbTiO_3$ та $SrZrO_3$ (001) для AO та BO_2 граничних поверхонь майже рівні. Навпаки, обчислені поверхневі енергії як для AO_3, так і для B граничних поверхонь (111) дуже відрізняються. Розраховані поверхневі енергії $SrTiO_3$, $BaTiO_3$, $PbTiO_3$ та $SrZrO_3$ (111) завжди значно більші за поверхневі енергії (001). Ковалентність хімічного зв'язку $SrTiO_3$, $BaTiO_3$, $PbTiO_3$ та $SrZrO_3$ об'ємного Ti-O (Zr-O) збільшується поблизу їхніх граничних поверхонь з BO_2 (001), а також з AO_3 (111). Обговорено систематичні тенденції в розрахунках для перовскітів $SrTiO_3$, $BaTiO_3$, $PbTiO_3$ та $SrZrO_3$, а також для об'ємних та (001) поверхневих *F*-центрів.

Ключові слова: *Ab initio* розрахунки, поверхні перовскіту ABO_3, B3PW, B3LYP, поверхневі енергії.